Review

Magnetic and Electric Properties of Organic Conductors Probed by ^{13}C-NMR Using Selective-Site Substituted Molecules

Shinji Hirose, Masaki Misawa and Atsushi Kawamoto *

Department of Condensed Matter Physics, Hokkaido University, Kita-ku Sapporo, Hokkaido 060-0810, Japan; E-Mails: saviour-oct-26@ec.hokudai.ac.jp (S.H.); Masaki.Misawa@jp.sony.com (M.M.)

* Author to whom correspondence should be addressed; E-Mail: atkawa@phys.sci.hokudai.ac.jp; Tel.: +81-01-706-4423; Fax: +81-01-706-4926.
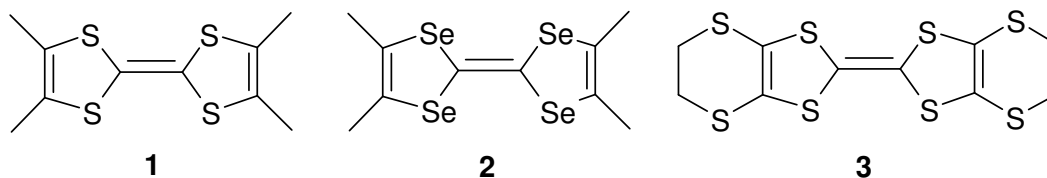
Abstract: Quasi-One and quasi-two dimensional organic conductors consisting of TTF derivatives such as BEDT-TTF (bis-(ethylene-dithio)-tetra-thia-fulvalene) and TMT*C*F (*C* = S; TMTTF: tetra-methyl-tetra-thia-fulvalene, C = Se; TMTSF: tetra-methyl-tetra-selena-fulvalene) have been well investigated in condensed matter physics because of interest in the emerging electric and magnetic properties, such as the spin density wave, charge order, superconductivity, anti-ferromagnetism, and so on. To probe the electronic state, nuclear magnetic resonance (NMR) is one of the most powerful tools as the microscopic magnetometer. A number of ^{13}C-NMR studies have been performed of the double-site central ^{13}C=^{13}C bond substituted molecules. However, problems with the coupled spin system of ^{13}C=^{13}C complicated the interpretation for observations on NMR. Therefore, single-site ^{13}C-enriched molecules are desired. We summarize the problem of Pake doublet and the preparation of the single-site ^{13}C-susbstituted BEDT-TTF and TMT*C*F molecules. We also demonstrate the superiority of ^{13}C-NMR of the single-site ^{13}C-susbstituted molecule utilizing the hyperfine coupling tensor.

Keywords: ^{13}C-NMR; TMTTF; TMTSF; BEDT-TTF; Pake doublet; hyperfine coupling tensor

1. Introduction

Organic conductors consisting of molecular donor and inorganic anion have been the subject of intense interest because of their low dimensionality, magnetism, and superconductivity [1–4]. Among them, (TMTCF)$_2$X (C = S; TMTTF: tetra-methyl-tetra-thia-fulvalene, C = Se; TMTSF: tetra-methyl-tetra-selena-fulvalene) salts are known as quasi-one dimensional organic conductors, and, moreover, (BEDT-TTF)$_2$X (BEDT-TTF: bis-(ethylene-dithio)-tetra-thia-fulvalene) salts are known as quasi-two dimensional organic conductors, where X$^-$ is a monovalent inorganic anion. Figure 1 shows the molecular structure of their donors. The electronic properties emerging in these salts can be controlled by applying pressure and chemical substitutions [5].

Figure 1. Molecular structures of tetra-methyl-tetra-thia-fulvalene (TMTTF), tetra-methyl-tetra-selena-fulvalene (TMTSF) and bis-(ethylene-dithio)-tetra-thia-fulvalene (BEDT-TTF).

Among (TMTSF)$_2$X, the so-called Bechgaard salt, (TMTSF)$_2$PF$_6$ is the first organic superconductor, and the superconductivity emerges at 1.6 K under pressure of 0.65~1 GPa [6]. In (TMTSF)$_2$ClO$_4$ which consists of the same donor molecule, the superconductivity emerges at 1.2 K at ambient pressure [7]. In TMTTF salt, (TMTTF)$_2$AsF$_6$ and (TMTTF)$_2$SbF$_6$ show charge ordered (CO) state below 100 K and 157 K, and theoretical and experimental studies have been performed from the view of the relationship between CO system and magnetism emerging at lower temperature [8–10]. Moreover, (TMTTF)$_2$Br shows commensurate antiferromagnetism below 13 K at ambient pressure [11]. With applying pressure over 0.5 GPa, the incommensurability of the magnetic state was suggested and discussed in relation to the spin density wave (SDW) in (TMTSF)$_2$PF$_6$ at ambient pressure [12]. The substitution of inorganic anions is considered to be due to the chemical pressure. The physical or chemical pressure dependence of the electronic properties was described by the universal phase diagram proposed by Jerome *et al.* [5].

On the other hand, the quasi-two dimensional organic conductor, (BEDT-TTF)$_2$X shows the various electronic properties according to the molecular arrangement. In κ-(BEDT-TTF)$_2$X, two BEDT-TTF molecules form a dimer, which constitutes the half-filled electronic system with the strongly-electron correlation. As a result, a similar competition occurs with adjacent and coexisting superconducting and antiferromagnetic phases as in high-T_c cuprates and heavy fermion systems at low temperatures [4,13,14]. Indeed, κ-(BEDT-TTF)$_2$Cu(NCS)$_2$ and κ-(BEDT-TTF)$_2$Cu[N(CN)$_2$]Br show superconductivity below 10.4 K and 11.6 K and κ-(BEDT-TTF)$_2$[N(CN)$_2$]Cl shows antiferromagnetic order below 27 K [15,16]. These electronic properties in κ-(BEDT-TTF)$_2$X are described in the phase diagram predicted by Kanoda *et al.*, in which the physical properties can be controlled by temperature, physical pressure, and chemical substitution parameters. Since the superconductivity is close to antiferromagnetism at low temperature, theoretical studies about electronic properties in

κ-(BEDT-TTF)$_2$X were performed from the viewpoint of the strongly-correlated electron system [17–21].

Salt with another packing arrangement, α-(BEDT-TTF)$_2$X and θ-(BEDT-TTF)$_2$X, has been a topic of interest due to the metal-insulator (MI) transition and charge disproportionation by off-site coulomb interaction [22–29]. In this type of organic conductor, various charge disproportionation patterns are realized, and these patterns give important information about the electronic structure. Recently, the mechanism of superconductivity by the charge fluctuation instability has also been intensively discussed [30–32].

Many theoretical and experimental studies of these interesting topics have been performed over the past three decades [33–35]. In order to reveal the electronic properties of (TMTCF)$_2$X and (BEDT-TTF)$_2$X from the microscopic view, Nuclear Magnetic Resonance (NMR) measurement is one of the most powerful tools. In ^{1}H-NMR, however, the spectrum showed no significant change due to the small hyperfine coupling constant and the large dipole–dipole interaction between [1]H-nuclei. Whereas the hyperfine coupling constant is large for [77]Se, there are four crystallographic independent [77]Se sites in a unit cell, and the four crystallographic independent [77]Se sites complicate the analysis of the spectrum in (TMTSF)$_2$X salt [36]. Moreover, there is no [77]Se site in TMTTF and BEDT-TTF. In contrast, ^{13}C-NMR shows sharp spectrum with large hyperfine coupling constant. In order to reveal the electronic properties, ^{13}C-NMR is suitable. However, most ^{13}C-NMR studies are performed on the double-side substituted central [13]C=[13]C in TTF skeleton because of the molecular symmetry of TTF derivatives. In the case of double-side enriched sample, two ^{13}C nuclei are coupled due to the dipole–dipole interaction and the spectrum starts to become complicated (the so called Pake doublet). Therefore, TMTCF and BEDT-TTF, in which one side of the central carbon bond is substituted with ^{13}C, are desired. In this paper, we first summarize the problem of Pake doublet, next we present the synthesis methods of single-site ^{13}C-substituted molecules which avoid the Pake doublet problem, and demonstrate the superiority of ^{13}C-NMR of these molecular crystals.

2. Problems of Pake Doublet

In case of the coupled spins system in the central [13]C=[13]C bond in TTF skeleton, the nuclear dipole–dipole interaction, $\hat{H}_{dip}$, is added to Zeeman interaction, $\hat{H}_{nZ}$. These interactions are described as,

$$\hat{H}_{nZ} = -g_N \mu_N H_0 (\hat{I}_{1z} + \hat{I}_{2z}) \tag{1}$$

$$\hat{H}_{dip} = \frac{g_N{}^2 \mu_N{}^2}{r^3} \left\{ \hat{\mathbf{I}}_1 \cdot \hat{\mathbf{I}}_2 - \frac{3(\hat{\mathbf{I}}_1 \cdot \mathbf{r})(\hat{\mathbf{I}}_2 \cdot \mathbf{r})}{r^2} \right\} \tag{2}$$

Here, $\hat{\mathbf{I}}_1$, $\hat{\mathbf{I}}_2$, g_N, H_0, μ_N, r are the spin operators of each nuclear site, the *g* factor of nuclei, the magnitude of the external magnetic field, the nuclear magneton, and the vector between two nuclei. This dipole–dipole interaction, $\hat{H}_{dip}$, can be expressed as, using $\hat{I}_{1(2)z}$ and the creation-annihilation operators, $\hat{I}_{1(2)}^{+(-)}$,

$$\hat{H}_{dip} = \frac{g_N^{\ 2}\mu_N^{\ 2}}{r^3}(A + B + C + D + E + F)$$

(3)

Here, *A~F* terms are defined as,

$$A = (1 - 3\cos^2\theta)\hat{I}_{1z}\hat{I}_{2z}$$

$$B = -\frac{1}{4}(1 - 3\cos^2\theta)\left(\hat{I}_1^+\hat{I}_2^- + \hat{I}_1^-\hat{I}_2^+\right)$$

$$C = -\frac{3}{2}\sin\theta\cos\theta e^{-i\phi}\left(\hat{I}_{1z}\hat{I}_2^+ + \hat{I}_1^+\hat{I}_{2z}\right)$$

$$D = -\frac{3}{2}\sin\theta\cos\theta e^{i\phi}\left(\hat{I}_{1z}\hat{I}_2^- + \hat{I}_1^-\hat{I}_{2z}\right)$$

$$E = -\frac{3}{4}\sin^2\theta e^{-2i\phi}\hat{I}_1^+\hat{I}_2^+$$

$$F = -\frac{3}{4}\sin^2\theta e^{2i\phi}\hat{I}_1^-\hat{I}_2^-$$

Here, θ is the angle between the external field and the direction of the central C=C bond. Since the terms of *A* and *B* are commutative with the nuclear Zeeman interaction, terms of *A* and *B* contribute to NMR shift, whereas other anticommutative terms act in the way of the second-order perturbation. Hence, the spin states of the coupled spin system are expressed as the triplet state,

$$\Psi_{1,1} = |\alpha\alpha\rangle, \quad E_{1,1} = -g_N\mu_N H_0 + \frac{g_N\mu_N H_0 d}{4}$$

(4)

$$\Psi_{1,0} = \frac{|\alpha\beta\rangle + |\beta\alpha\rangle}{\sqrt{2}}, \quad E_{1,0} = -\frac{g_N\mu_N H_0 d}{2}$$

(5)

$$\Psi_{1,-1} = |\beta\beta\rangle, \quad E_{1,-1} = g_N\mu_N H_0 + \frac{g_N\mu_N H_0 d}{4}$$

(6)

and the singlet state,

$$\Psi_{0,0} = \frac{|\alpha\beta\rangle - |\beta\alpha\rangle}{\sqrt{2}}, \quad E_{0,0} = 0$$

(7)

Here, $d = g_N\mu_N(1 - 3\cos^2\theta)/H_0 r$. As a result, the two transitions of $\Delta E_{1,1\leftrightarrow 0} = g_N\mu_N H_0(1 - 3d/4)$ and $\Delta E_{1,0\leftrightarrow -1} = g_N\mu_N H_0(1 + 3d/4)$ between closest levels in the triplet state are allowed with same intensities. This doublet structure is the so called Pake doublet.

In realistic TMTC*F* and BEDT-TTF compounds, the situation is more complicated. Generally, two nuclei in $^{13}C = ^{13}C$ bond are crystallographic nonequivalent even in symmetrical molecule. Defining NMR shifts at two local sites as δ_1 and δ_2, the nuclear Zeeman interaction, $\hat{H}_{nZ}$, is modified as,

$$\hat{H}_{nZ} = -g_N \mu_N H_0 \left\{ (1+\delta_1)\hat{I}_{1z} + (1+\delta_2)\hat{I}_{2z} \right\} \tag{8}$$

and the energy matrix is expressed as,

$$\langle \Psi | \hat{H}_n | \Psi \rangle = \begin{bmatrix} \langle \Psi_{1,1} | \hat{H}_n | \Psi_{1,1} \rangle & \langle \Psi_{1,1} | \hat{H}_n | \Psi_{1,0} \rangle & \langle \Psi_{1,1} | \hat{H}_n | \Psi_{1,-1} \rangle & \langle \Psi_{1,1} | \hat{H}_n | \Psi_{0,0} \rangle \\ \langle \Psi_{1,0} | \hat{H}_n | \Psi_{1,1} \rangle & \langle \Psi_{1,0} | \hat{H}_n | \Psi_{1,0} \rangle & \langle \Psi_{1,0} | \hat{H}_n | \Psi_{1,-1} \rangle & \langle \Psi_{1,0} | \hat{H}_n | \Psi_{0,0} \rangle \\ \langle \Psi_{1,-1} | \hat{H}_n | \Psi_{1,1} \rangle & \langle \Psi_{1,-1} | \hat{H}_n | \Psi_{1,0} \rangle & \langle \Psi_{1,-1} | \hat{H}_n | \Psi_{1,-1} \rangle & \langle \Psi_{1,-1} | \hat{H}_n | \Psi_{0,0} \rangle \\ \langle \Psi_{0,0} | \hat{H}_n | \Psi_{1,1} \rangle & \langle \Psi_{0,0} | \hat{H}_n | \Psi_{1,0} \rangle & \langle \Psi_{0,0} | \hat{H}_n | \Psi_{1,-1} \rangle & \langle \Psi_{0,0} | \hat{H}_n | \Psi_{0,0} \rangle \end{bmatrix}$$

$$= \begin{bmatrix} -g_N\mu_N H_0(1+\delta_{AV}-d/4) & 0 & 0 & 0 \\ 0 & -g_N\mu_N H_0 d/2 & 0 & -g_N\mu_N H_0 \Delta\delta/2 \\ 0 & 0 & g_N\mu_N H_0(1+\delta_{AV}+d/4) & 0 \\ 0 & -g_N\mu_N H_0 \Delta\delta/2 & 0 & 0 \end{bmatrix} \tag{9}$$

Here, $\Delta\delta$ and δ_{AV} are the difference and the average of NMR shift between two local sites, respectively. Because of the off-diagonal elements in the energy matrix, the hybridization between the singlet and triplet states occurs and the eigenstates are expressed as follow,

$$\Psi_A = \Psi_{1,1}, \quad E_A = -g_N\mu_N H_0 \left(1+\delta_{AV} - \frac{d}{4} \right) \tag{10}$$

$$\Psi_B = \frac{1}{\sqrt{1+\left(d+\sqrt{d^2+4\Delta\delta^2}/2\Delta\delta\right)^2}} \left(\frac{d+\sqrt{d^2+4\Delta\delta^2}}{2\Delta\delta} \Psi_{1,0} + \Psi_{0,0} \right)$$

$$E_B = -\frac{g_N\mu_N H_0}{4}\sqrt{d^2+4\Delta\delta^2} - \frac{g_N\mu_N H_0 d}{4} \tag{11}$$

$$\Psi_C = \Psi_{1,-1}, \quad E_C = g_N\mu_N H_0 \left(1+\delta_{AV} + \frac{d}{4} \right) \tag{12}$$

$$\Psi_D = \frac{1}{\sqrt{1+\left(d-\sqrt{d^2+4\Delta\delta^2}/2\Delta\delta\right)^2}} \left(\frac{d-\sqrt{d^2+4\Delta\delta^2}}{2\Delta\delta} \Psi_{1,0} + \Psi_{0,0} \right)$$

$$E_D = \frac{g_N\mu_N H_0}{4}\sqrt{d^2+4\Delta\delta^2} - \frac{g_N\mu_N H_0 d}{4} \tag{13}$$

As a consequence, all transitions between levels except that between Ψ_A and Ψ_C are allowed and we can observed four transitions,

$$\Delta E_{A \leftrightarrow B} = g_N\mu_N H_0 \left(1+\delta_{AV} - \frac{d}{2} - \frac{\sqrt{d^2+4\Delta\delta^2}}{4} \right) \tag{14}$$

$$\Delta E_{A \leftrightarrow D} = g_N\mu_N H_0 \left(1+\delta_{AV} - \frac{d}{2} + \frac{\sqrt{d^2+4\Delta\delta^2}}{4} \right) \tag{15}$$

$$\Delta E_{B \leftrightarrow C} = g_N \mu_N H_0 \left(1 + \delta_{AV} + \frac{d}{2} + \frac{\sqrt{d^2 + 4\Delta\delta^2}}{4} \right) \tag{16}$$

$$\Delta E_{C \leftrightarrow D} = g_N \mu_N H_0 \left(1 + \delta_{AV} + \frac{d}{2} - \frac{\sqrt{d^2 + 4\Delta\delta^2}}{4} \right) \tag{17}$$

These transitions are categorized into two groups with different intensities. One group is an outside pair of the quartet (O), the other group is an inside pair of the quartet (I). These shifts, $\delta_{\pm}^{O(I)}$, and intensities, $I^{O(I)}$, are expressed as,

$$\delta_{\pm}^{O} = \delta_{AV} \pm \left\{ \frac{d}{2} + \sqrt{\frac{d^2}{16} + \frac{\Delta\delta^2}{4}} \right\}, \quad I^{O} \propto 1 + \frac{1}{\sqrt{1 + 4(\Delta\delta/d)^2}} \tag{18}$$

$$\delta_{\pm}^{I} = \delta_{AV} \pm \left\{ \frac{d}{2} - \sqrt{\frac{d^2}{16} + \frac{\Delta\delta^2}{4}} \right\}, \quad I^{I} \propto 1 - \frac{1}{\sqrt{1 + 4(\Delta\delta/d)^2}} \tag{19}$$

respectively. In π electron system, $\delta_{1(2)}$ depends on the direction of the external field to the crystal system, and the angular dependence of $\delta_{1(2)}$ around a rotational axis shows a simple sinusoidal curve. However, As $\delta_{\pm}^{O(I)}$ also depends on the angle of θ, the angular dependence of $\delta_{\pm}^{O(I)}$ does not show a simple curve but a complicated one.

In the limit of $\Delta\delta \gg d$, the mean values of two higher (lower) shift in quartet represent NMR shift at two local sites,

$$\frac{\delta_{+}^{O} + \delta_{-}^{I}}{2} = \delta_1 + \delta_2 + \sqrt{\frac{d^2}{4} + \Delta\delta^2} \xrightarrow{\Delta\delta \gg d} \delta_1 \tag{20}$$

$$\frac{\delta_{-}^{O} + \delta_{+}^{I}}{2} = \delta_1 + \delta_2 - \sqrt{\frac{d^2}{4} + \Delta\delta^2} \xrightarrow{\Delta\delta \gg d} \delta_2 \tag{21}$$

Whereas, the mean value does not represent the shift of the local nucleus in the case of $\Delta\delta \approx d$. Since the spin susceptibility is connected to NMR shift at local nucleus via hyperfine coupling constant, NMR shift does not represent the local spin susceptibility. Since the magnitude of d is proportional to H_0^{-1}, the problems actually surface in the low field experiments, such as that under superconductivity.

The mixing of $|\alpha\beta\rangle$ and $|\beta\alpha\rangle$ depending on the parameter of $\Delta\delta$ also have an influence on the spin-lattice relaxation time, T_1, which intrinsically depends on the magnetic fluctuation at each local nucleus. Therefore, the relaxation to the mixing states is driven by the magnetic fluctuation on both sites, and the problems of Pake doublet causes great loss of the advantage of the local magnetic probe.

In the coupled spin system in the double-side ^{13}C-substituted molecules, the transverse nuclear magnetization induced by RF pulse is always modulated by $\hat{H}_{dip}$, which cannot be canceled by the spin echo, $\pi/2$-π pulse, sequence. Therefore, the spectrum by the fast Fourier transformation of this modulated spin echo signal contains the spurious information such as the negative intensity [37]. This modulation could be canceled by the solid echo pulse sequence [38]. There are a few experiments using solid echo pulse sequence [39]. However, this sequence requires the fast recovery RF system and

restricts the advantage of the conventional spin echo. This modulation also inhibits the measurement of the spin-spin relaxation time, T_2. There are some estimations of T_2 deduced from the envelope of the modulated spin echo intensity, so called *J*-modulation [40,41]. However, this method estimates T_2 for overall spectrum in the coupled spin system and is not conventional.

In condensed matter physics, NMR measurement is one of the most powerful tools as the magnetometer on the specific local site. However, the coupled spin system of the double-side substituted molecule modulates NMR spectrum, mixes local spin states, and weakens the character as the local magnetic probe. The magic angle setting $(1 - 3\cos^2\theta = 0)$ is one of alternative methods to avoid Pake doublet problem [8,42]. However, the setting restricts the direction of the external field. Therefore, the single-site substituted TMT*CF* and BEDT-TTF are desired.

3. Synthetic Method of Single-Site ^{13}C- Substituted Molecule

In preparing the single-site substituted T*CF* derivatives, a candidate reaction is the cross-coupling of a ketone and a thioketone. Figure 2 shows the use of this method to prepare one-side enriched BEDT-TTF [43]. Thioketone-Ketone coupling takes precedence over any self-coupling. We found that the treatment of the ketone-*d*4 and the thioketone-*d*0 with triethyl phosphite mainly produced BEDT-TTF-*d*4 with the minor product of BEDT-TTF-*d*8 and the trace amount of BEDT-TTF-*d*0 with a ratio of 0.7:0.24:0.06 from mass spectroscopy. Thus, the reaction of an enriched thioketone and non-enriched ketone produces ^{13}C=^{12}C molecule as major products, ^{12}C=^{12}C molecule as minor product, and ^{13}C=^{13}C molecule in only trace amounts. For ^{13}C-NMR spectral purposes, the contamination by the inactive ^{12}C=^{12}C is unimportant, and it is important to prevent the contamination of the ^{13}C=^{13}C molecule which superimposes on the additional modulated resonance line. Indeed as shown in Figure 3, there are four magnetically independent central C=C sites, A-a, A-b, B, and C in the NMR spectra of α-(BEDT-TTF)$_2$I$_3$ without other additional peaks from ^{13}C=^{13}C molecule.

Figure 2. Cross-Coupling reaction of a ketone and a thioketone for BEDT-TTF.
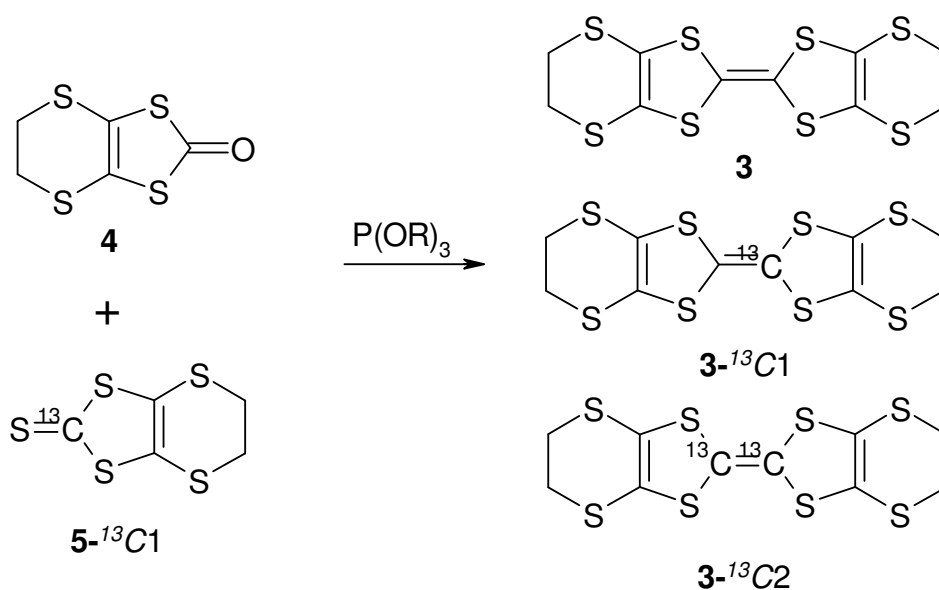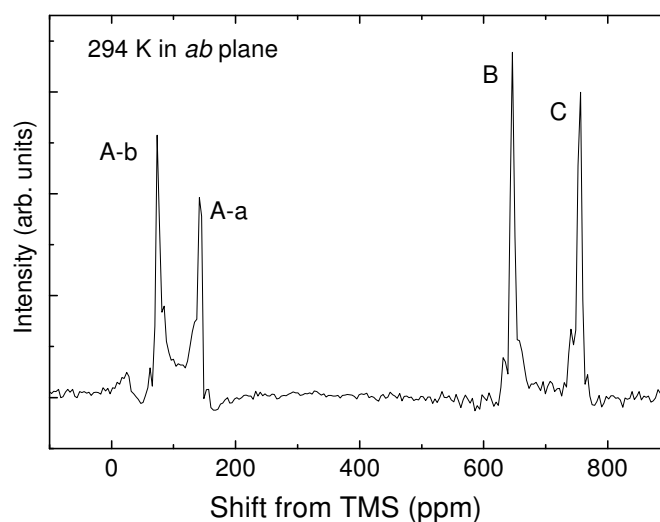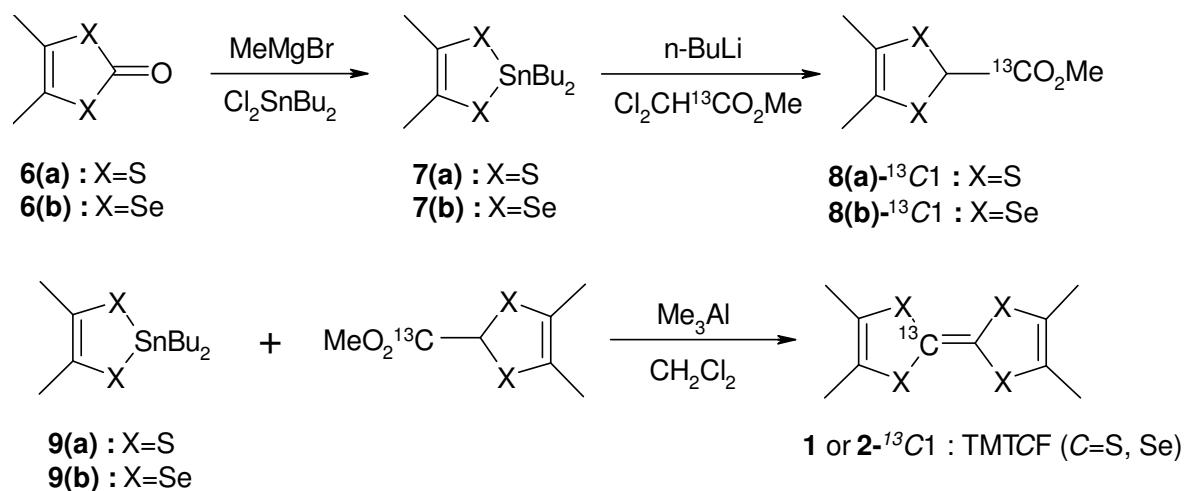
Figure 3. ^{13}C-NMR spectra for α-(BEDT-TTF)$_2$I$_3$.
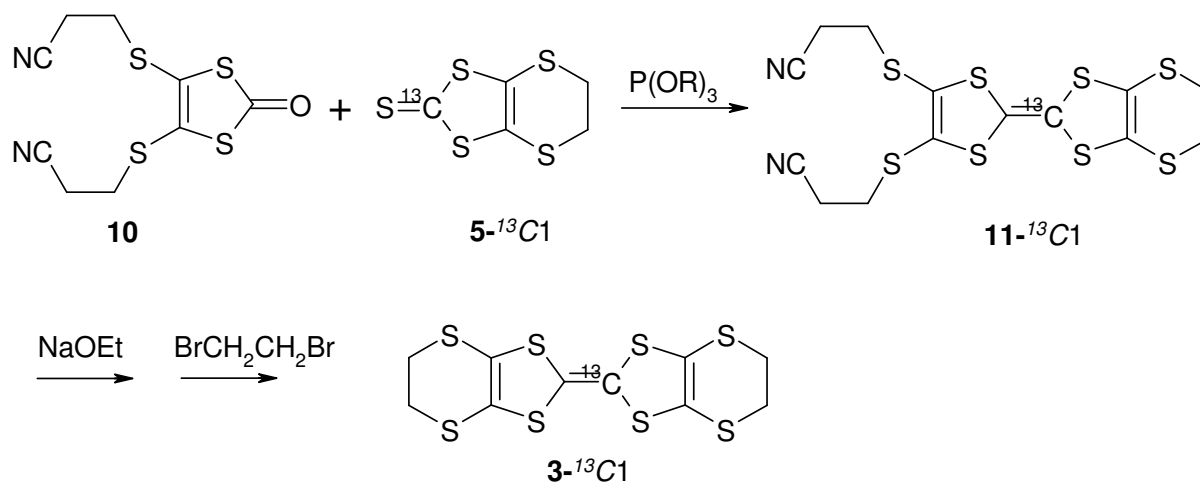
In the traditional coupling method [43], TMTTF is prepared from ^{13}CS$_2$ as the starting material. However, we could obtain the stochastically or 100% double-side ^{13}C-enriched TMTTF. For TMTSF, problems exist with the availability of the starting isotope reagent, (CH$_3$)$_2$N^{13}CCl$_2$Cl [44], or ^{13}CSe$_2$ [45], and we also obtain stochastically or 100% double-side ^{13}C-enriched TMTSF. In a previous study [11], Barthel and Bechgaard *et al.* obtained ^{13}C-NMR spectra of (TMTSF)$_2$PF$_6$ using stochastically 10% ^{13}C-enriched molecules, but the low isotope ratio worsened the signal-to-noise ratio and restricted the measurement temperature. In the end, we could not produce TMTTF by couplings ketones, and the stochastic coupling of the corresponding carbene resulted in the contamination of the stochastic ^{13}C=^{13}C-enriched molecule. For TMTSF, the hetero-coupling has not been studied, and the problem of the starting material remains.

Because the well-established synthetic route to prepare TMT*C*F is not suitable for the isotope substitution, we explored an alternative procedure. The single-site ^{13}C-substituted molecule is an unsymmetrical donor. Among the synthetic routes to prepare unsymmetrical donors, those used as symmetrical donor have not yet been considered, but may be worth consideration in the future. Figure 4 shows one such candidate, the synthetic route of Yamada *et al.* using dibutyltin complex [46]. Advantages of this method are that the isotope reagent dichloroacetic acid methyl ester is available and that Yamada *et al.* have already established the precursors of 8 and 9.

We synthesized the one-side ^{13}C-enriched TMT*C*F by Yamada's method and characterized the products by mass spectroscopy and ^{1}H-NMR. The yields with respect to the starting reagent dichloroacetic acid methyl ester were 10% for TMTTF [47], and 3% for TMTSF [48]. Compared to yields obtained by the traditional method, these yields are low. However, the method enables the preparation of enriched radical salts using the conventional electrochemical cell, and may be useful for preparing other enriched donor molecules as well.
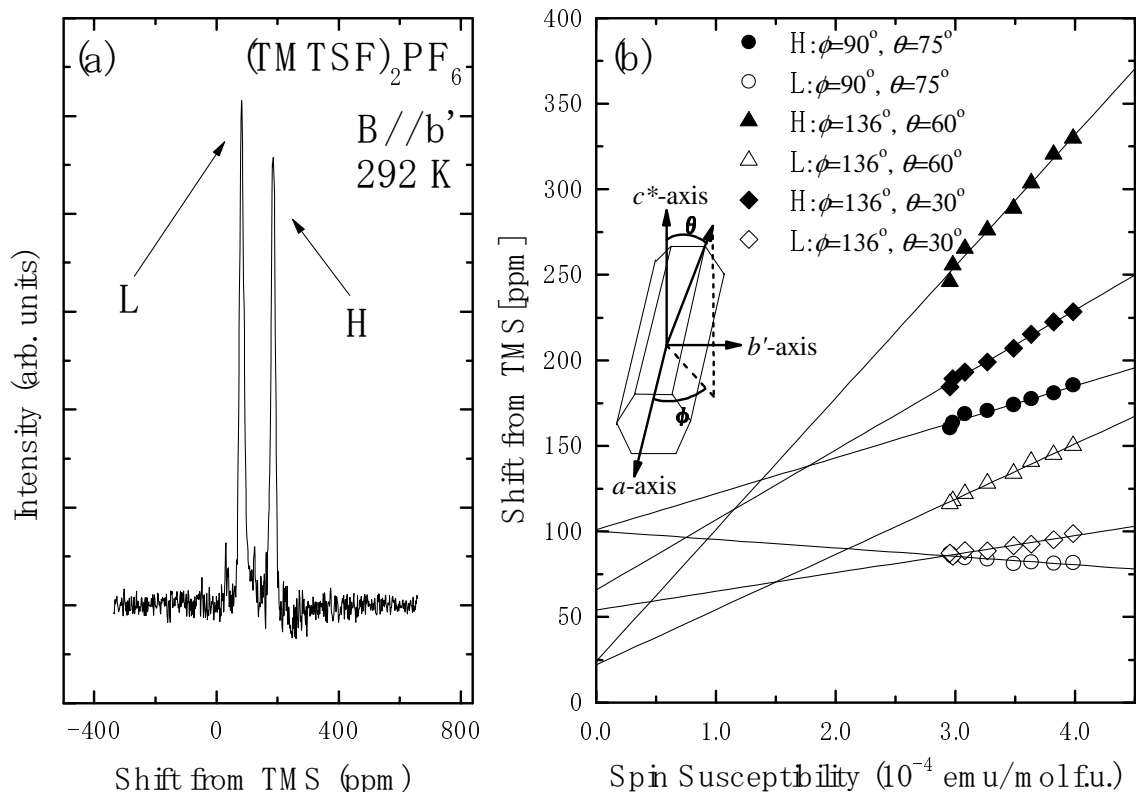
Figure 4. Synthetic route to prepare one-side ^{13}C-enriched TMTCF.

6(a) : X=S
6(b) : X=Se

7(a) : X=S
7(b) : X=Se

8(a)-^{13}C1 : X=S
8(b)-^{13}C1 : X=Se

9(a) : X=S
9(b) : X=Se

1 or **2**-^{13}C1 : TMTCF (*C*=S, Se)

We also made an attempt to synthesize for the selective one-side enriched BEDT-TTF by this method. Unfortunately, the yield discourages practical use. Then we explored one of the alternatives with the precursor of **11** shown in Figure 5 [49]. After purification, we obtained the selective one-side enriched BEDT-TTF with a yield of 36% based on **11** [50].

Figure 5. Synthetic route to prepare selective one-side ^{13}C-enriched BEDT-TTF.

10

5-^{13}C1

11-^{13}C1

3-^{13}C1

To demonstrate the suitability for ^{13}C-NMR spectral purposes of enriched molecules thus prepared, we synthesized a single crystal of (TMTSF)$_2$PF$_6$ and examined its spectrum. Figure 6a shows the ^{13}C-NMR spectrum for (TMTSF)$_2$PF$_6$ at 292 K [51]. There are two crystallographically non-equivalent ^{13}C sites in (TMTCF)$_2$X salts. Hence it is expected that two peaks are observed in metallic state, and we actually observed only two peaks. The linewidth of about 30 ppm is very sharp and the small variation of NMR shift can be detected. Signal-to-Noise ratio is sufficient even at room temperature, and we can measure from room temperature.

Figure 6. (**a**) ^{13}C-NMR spectrum for (TMTSF)$_2$PF$_6$ at 292 K; (**b**) χ-δ plot in the metallic phase of (TMTSF)$_2$PF$_6$ at several angles [51].

4. NMR Investigation Utilizing Hyperfine Coupling and Chemical Shift Tensor

4.1. NMR Shift on Molecular Conductors

The NMR shift δ can be expressed as $\delta = \sigma + K = \sigma + A\chi_s$. Here σ is chemical shift, and K is Knight shift. A is the hyperfine coupling constant, and χ_s is the spin susceptibility. Chemical shift is caused by the orbital current and is expressed as tensor, σ, due to crystal anisotropy in solid. Ignoring the small effect of the ring current of surrounding molecules, chemical shift depends on the electron orbital on on-site molecule, $\square_i$, and is expressed as,

$$\sigma_{zz} = \frac{e\hbar}{2mc}\sum_i \left\langle \phi_i \left| 2\frac{L_z}{r^3} \right| \phi_i \right\rangle - \frac{e^2}{2mc^2}\sum_i \left\langle \phi_i \left| \frac{x^2 + y^2}{r^3} \right| \phi_i \right\rangle \tag{22}$$

Here, m, c, e, L_z are the electron mass, velocity of light, electron charge and operator of the angular momentum. The summation is performed over all occupied orbitals. Dividing the summation into the valence (core) and highest (lowest) occupied (unoccupied) molecular orbital, HOMO (LUMO) parts, the chemical shift can be expressed as,

$$\sigma_{zz} = \sigma_{zz,core} + \frac{e\hbar}{2mc}\sum_{E_k \leq E_F} \left\langle \varphi_k \left| 2\frac{L_z}{r^3} \right| \varphi_k \right\rangle - \frac{e^2}{2mc^2}\sum_{E_k \leq E_F} \left\langle \varphi_k \left| \frac{x^2 + y^2}{r^3} \right| \varphi_k \right\rangle \tag{23}$$

Here, the summation is performed below Fermi energy, and φ_k is the Bloch wave function constructed from HOMO (LUMO) on molecules in a crystal and is expressed as,

$$\varphi_k = \frac{1}{\sqrt{N}} \sum_n c_{k,n} \phi_{HOMO}(\mathbf{r} - \mathbf{R}_n) \tag{24}$$

Here, $\mathbf{R}_n$ is the translation vector in the crystal. From the second perturbation, the matrix element of the second term is represented by the excited state, $\square_n^0$, as,

$$\frac{e\hbar}{2mc}\left\langle \varphi_k \left| \frac{2L_z}{r^3} \right| \varphi_k \right\rangle = \left(\frac{e\hbar}{2mc}\right)^2 |c_{k,0}|^2 \sum_n \frac{\left\langle \phi_{HOMO} \left| L_z \right| \phi_n^0 \right\rangle \left\langle \phi_n^0 \left| \frac{2L_z}{r^3} \right| \phi_{HOMO} \right\rangle}{E_n - E_{HOMO}} + c.c. \tag{25}$$

In transition metals, the excitation energy, E_n-E_{HOMO}, corresponds to small ligand field splitting energy and this term becomes important. Whereas, in planer organic conductors, the excited state, $\square_n^0$, corresponds to the sp^2-hybrided σ^* orbital, and the excited energy is large, and the chemical shift is simplified as,

$$\sigma_{zz} = \sigma_{zz,core} - \frac{e^2}{2mc^2}\left\langle \phi_{HOMO} \left| \frac{x^2 + y^2}{r^3} \right| \phi_{HOMO} \right\rangle \sum_{E_k \leq E_F} |c_{k,0}|^2 \tag{26}$$

Therefore, the chemical shift depends on the molecular structure. The summation part depends on the degree of the band filling and the chemical shift can probe the charge on the molecule.

Knight shift, K, has the contributions from the core polarization and the dipole field and is proportional to on-site local spin susceptibility, χ_{local}, described as,

$$\chi_{local} = \left| \left\langle \varphi_{k_F} \left| \phi_{HOMO} \right\rangle \right|^2 \chi_s = |c_{k_F,0}|^2 \chi_s \tag{27}$$

The hyperfine coupling constant by this contribution can be expressed as the tensor, $\mathbf{A}_0$, and depends on the molecular structure similar to chemical shift. In addition, however, there are the dipole interaction and exchange interaction from the neighboring molecules. The exchange term between molecules depends on the transfer integral between molecules and is sensitive to the topology of the band structure. In this case, the Knight shift can be expressed as a summation of on-site and off-site molecular contributions. When the hyperfine coupling tensor by the dipole interaction and exchange interaction from off-site molecule is given as $\mathbf{B}_i$, the hyperfine coupling tensor, $\mathbf{A}$, can be expressed as

$$K = \tilde{\mathbf{h}}\mathbf{A}_0\mathbf{h}\chi_{local} + \sum_i \tilde{\mathbf{h}}\mathbf{B}_i\mathbf{h}\chi_{local} = \tilde{\mathbf{h}}\left(\mathbf{A}_0 + \sum_i \mathbf{B}_i\right)\mathbf{h}\chi_{local} = \tilde{\mathbf{h}}\mathbf{A}\mathbf{h}\chi_{local} \tag{28}$$

Here, $\mathbf{h}$ is a direction cosine of the external field. Namely, observed hyperfine coupling constant is modified by the crystal and band structure and the off-site hyperfine coupling tensor, $\mathbf{B}_i$, and depends on molecular location in spite of the isomorphic molecular structure. Note that the chemical shift probes the summation of the projective coefficient blow Fermi energy, whereas the Knight shift probes the projective coefficient at Fermi energy.
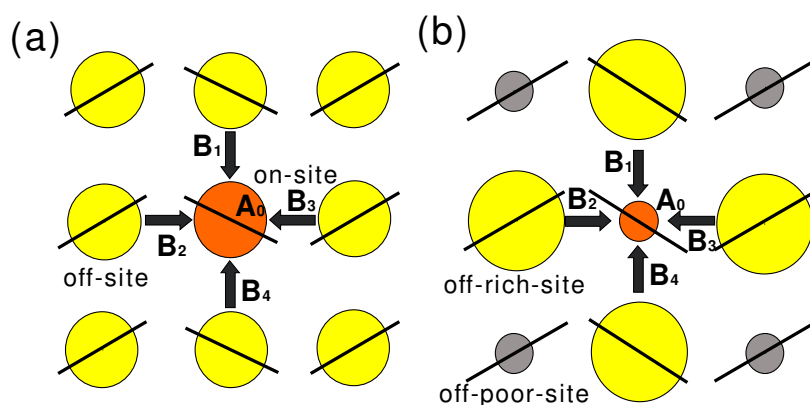
The problem is the case of the disproportionation between molecular sites in paramagnetic state. By this disproportionation of the local spin susceptibility, on-site and off-site hyperfine coupling tensors, $\mathbf{A}_0$ and $\mathbf{B}_i$, does not change but Knight shift in spin-rich and spin-poor sites, which is shown in Figure 7b, are described as,

$$K_{poor} = \tilde{\mathbf{h}}\mathbf{A}_0\mathbf{h}\chi_{poor} + \sum_i \tilde{\mathbf{h}}\mathbf{B}_i\mathbf{h}\chi_{rich}$$

(29)

$$K_{rich} = \tilde{\mathbf{h}}\mathbf{A}_0\mathbf{h}\chi_{rich} + \sum_i \tilde{\mathbf{h}}\mathbf{B}_i\mathbf{h}\chi_{poor}$$

(30)
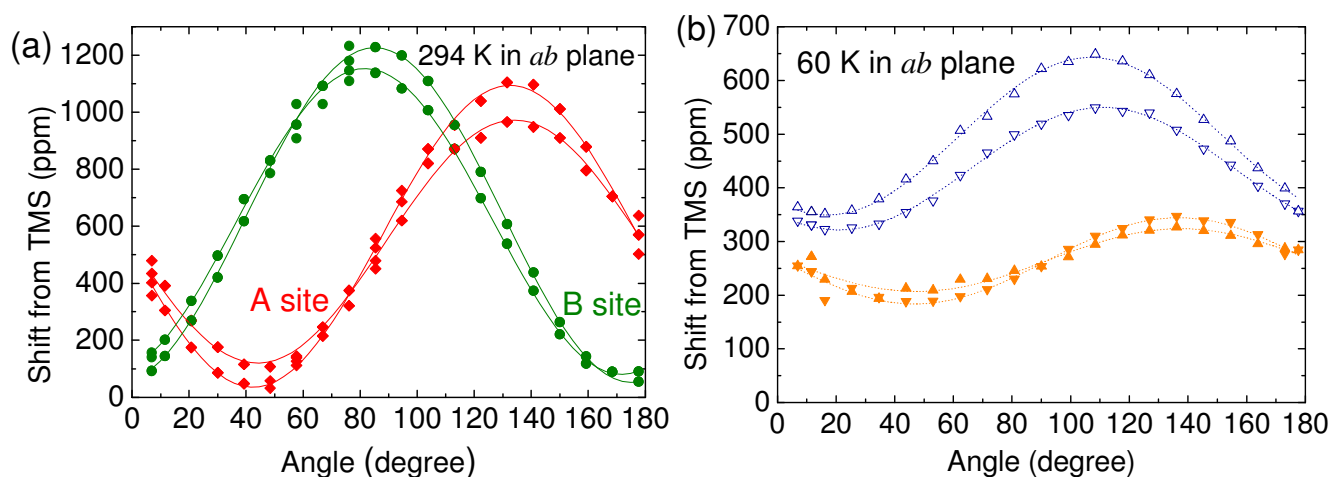
respectively. Here χ_{poor} and χ_{rich} are the local spin susceptibility on the spin-poor site and spin-rich site. In case of $\chi_{poor} \ll \chi_{rich}$, the Knight shift intensively depends on off-site hyperfine coupling tensor, $\mathbf{B}_i$, and becomes different from the regular state. Figure 8 show the angular dependence of NMR shift at 294 K and 60 K in ^{13}C NMR of α'-(BEDT-TTF)$_2$IBr$_2$, in which the charge order transition with the large disproportionation occurs below 200 K [52]. At 294 K, the principal axis of NMR shift tensor behave in unison with that of molecular orientation, which means the NMR shift mainly depends on on-site hyperfine coupling tensor, $\mathbf{A}$. In contrast, NMR shift at 60 K shows the different angular dependence from each molecular orientation. Previous NMR studies on large charge disproportionate salts were analyzed with the assumption that Knight shift was proportional to on-site susceptibility [28,53]. However, the off-site contribution is fundamental to the quantitative analysis on large charge disproportionate salts.

Figure 7. Schematic view of hyperfine coupling field around the neighboring molecules (**a**) in no disproportionation (**b**) in disproportionation of diagonal stripe pattern with on-site spin poor site. Here $\mathbf{A}_0$ and $\mathbf{B}_i$ ($i = 1, 2, 3, 4$) are the on-site and off-site hyperfine coupling fields. [52]

For diamagnetic organic materials, Knight shift diminishes and NMR shift corresponds to σ. For organic conductors, Knight shift involves the information of the spin susceptibility, and NMR is regarded as the microscopic magnetometer at enriched site. Because of the dipole and exchange field of the spin magnetization, Knight shift and the hyperfine coupling constant strongly depend on its crystal structure. In contrast, the chemical shift detects the shielding current around local nucleus and mainly depends on only its molecular structure. Hence, the chemical shift tensors of both central C=C sites are almost the same. To utilize the feature as the microscopic magnetometer, we must evaluate the hyperfine coupling constant and chemical shift. In π electron system, because of the molecular anisotropy, A and σ is expressed by the hyperfine coupling tensor $\mathbf{A}$ and chemical shift tensor $\boldsymbol{\sigma}$ as, $A = \tilde{\mathbf{h}}\mathbf{A}\mathbf{h}$, $\sigma = \tilde{\mathbf{h}}\boldsymbol{\sigma}\mathbf{h}$.

Figure 8. (**a**) Angular dependence of NMR shift at A and B local molecular sites at 294 K in *ab* plane rotation in *α'*-(BEDT-TTF)$_2$IBr$_2$; (**b**) Angular dependence of NMR shift at A and B local spin-poor molecular sites at 60 K in *ab* plane rotation in *α'*-(BEDT-TTF)$_2$IBr$_2$. At 60 K, The principal axes of NMR shift are intensively different from that at 294 K for large disproportionation of spin susceptibility [52].

4.2. Determination of the Hyperfine Coupling and Chemical Shift Tensor

We measured the temperature dependence of the NMR shift δ at several angles. From the slope of χ-δ plot as shown in Figure 6b, we could determine the hyperfine coupling constant A and chemical shift σ. Using these values at several angles, we determined hyperfine coupling tensors and chemical shift tensor as,

$$\mathbf{A}_H = \begin{pmatrix} \mathbf{A}_{aa} & \mathbf{A}_{ab'} & \mathbf{A}_{ac*} \\ \mathbf{A}_{b'a} & \mathbf{A}_{b'b'} & \mathbf{A}_{b'c*} \\ \mathbf{A}_{c*a} & \mathbf{A}_{c*b'} & \mathbf{A}_{c*c*} \end{pmatrix}_H = \begin{pmatrix} 9.0(4) & 0.0(1) & 0.3(2) \\ 0.0(1) & 1.08(8) & 0.21(7) \\ 0.3(2) & 0.21(7) & 1.42(4) \end{pmatrix} \ (\text{kOe}/\mu_{\mathbf{B}}) \tag{31}$$

$$\mathbf{A}_L = \begin{pmatrix} \mathbf{A}_{aa} & \mathbf{A}_{ab'} & \mathbf{A}_{ac*} \\ \mathbf{A}_{b'a} & \mathbf{A}_{b'b'} & \mathbf{A}_{b'c*} \\ \mathbf{A}_{c*a} & \mathbf{A}_{c*b'} & \mathbf{A}_{c*c*} \end{pmatrix}_L = \begin{pmatrix} 5.0(2) & 0.1(2) & 0.4(3) \\ 0.1(2) & -0.46(7) & 0.27(5) \\ 0.4(3) & 0.27(5) & 0.08(4) \end{pmatrix} \ (\text{kOe}/\mu_{\mathbf{B}}) \tag{32}$$

$$\boldsymbol{\sigma} = \begin{pmatrix} \boldsymbol{\sigma}_{aa} & \boldsymbol{\sigma}_{ab'} & \boldsymbol{\sigma}_{ac*} \\ \boldsymbol{\sigma}_{b'a} & \boldsymbol{\sigma}_{b'b'} & \boldsymbol{\sigma}_{b'c*} \\ \boldsymbol{\sigma}_{c*a} & \boldsymbol{\sigma}_{c*b'} & \boldsymbol{\sigma}_{c*c*} \end{pmatrix} = \begin{pmatrix} -80(10) & 0(10) & -20(10) \\ 0(10) & 118(1) & -30(1) \\ -20(10) & -30(1) & 82(6) \end{pmatrix} \ (\text{ppm}) \tag{33}$$

respectively [51]. We also prepared the single crystal of (TMTTF)$_2$Br and performed the same examination for the determination of the hyperfine coupling and chemical shift tensors. These results are listed as,

$$\mathbf{A}_H = \begin{pmatrix} \mathbf{A}_{aa} & \mathbf{A}_{ab'} & \mathbf{A}_{ac*} \\ \mathbf{A}_{b'a} & \mathbf{A}_{b'b'} & \mathbf{A}_{b'c*} \\ \mathbf{A}_{c*a} & \mathbf{A}_{c*b'} & \mathbf{A}_{c*c*} \end{pmatrix}_H = \begin{pmatrix} 8.04(7) & 0.29(8) & 0.43(8) \\ 0.29(8) & -0.3(1) & 0.03(8) \\ 0.43(8) & 0.03(8) & 0.06(8) \end{pmatrix} \ (\text{kOe}/\mu_{\mathbf{B}}) \tag{34}$$

$$\mathbf{A}_L = \begin{pmatrix} \mathbf{A}_{aa} & \mathbf{A}_{ab'} & \mathbf{A}_{ac*} \\ \mathbf{A}_{b'a} & \mathbf{A}_{b'b'} & \mathbf{A}_{b'c*} \\ \mathbf{A}_{c*a} & \mathbf{A}_{c*b'} & \mathbf{A}_{c*c*} \end{pmatrix}_L = \begin{pmatrix} 4.39(6) & 0.06(7) & 0.30(7) \\ 0.06(7) & -0.46(7) & 0.04(7) \\ 0.30(7) & 0.04(7) & 0.15(4) \end{pmatrix} \; (\text{kOe}/\mu_B) \tag{35}$$

$$\boldsymbol{\sigma} = \begin{pmatrix} \boldsymbol{\sigma}_{aa} & \boldsymbol{\sigma}_{ab'} & \boldsymbol{\sigma}_{ac*} \\ \boldsymbol{\sigma}_{b'a} & \boldsymbol{\sigma}_{b'b'} & \boldsymbol{\sigma}_{b'c*} \\ \boldsymbol{\sigma}_{c*a} & \boldsymbol{\sigma}_{c*b'} & \boldsymbol{\sigma}_{c*c*} \end{pmatrix} = \begin{pmatrix} -42(6) & 8(7) & -28(7) \\ 8(7) & 124(9) & -9(8) \\ -28(7) & -9(8) & 63(7) \end{pmatrix} \; (\text{ppm}) \tag{36}$$

As (TMTCF)$_2$X salts display the same isomorphism, it is reasonable that the results of (31)~(33) and (34)~(36) are nearly same.

We also determined the hyperfine coupling tensors of β'-(BEDT-TTF)$_2$ICl$_2$ from χ-δ plot as,

$$\mathbf{A}_{outer} = \begin{pmatrix} \mathbf{A}_{a*a*} & \mathbf{A}_{a*b'} & \mathbf{A}_{a*c} \\ \mathbf{A}_{b'a*} & \mathbf{A}_{b'b'} & \mathbf{A}_{b'c} \\ \mathbf{A}_{ca*} & \mathbf{A}_{cb'} & \mathbf{A}_{cc} \end{pmatrix}_{outer} = \begin{pmatrix} 4.2 & 3.8 & 0.12 \\ 3.8 & 2.5 & 0.60 \\ 0.12 & 0.60 & -0.84 \end{pmatrix} \; (\text{kOe}/\mu_B) \tag{37}$$

$$\mathbf{A}_{inner} = \begin{pmatrix} \mathbf{A}_{a*a*} & \mathbf{A}_{a*b'} & \mathbf{A}_{a*c} \\ \mathbf{A}_{b'a*} & \mathbf{A}_{b'b'} & \mathbf{A}_{b'c} \\ \mathbf{A}_{ca*} & \mathbf{A}_{cb'} & \mathbf{A}_{cc} \end{pmatrix}_{inner} = \begin{pmatrix} 0.56 & 2.3 & 0.08 \\ 2.3 & 1.8 & 0.70 \\ 0.08 & 0.70 & -1.5 \end{pmatrix} \; (\text{kOe}/\mu_B) \tag{38}$$

Here, inner and outer sites mean two crystallographic nonequivalent sites in a dimer of two BEDT-TTF molecules and b' axis is corresponded to the direction perpendicular to $ac*$ plane [54].

4.3. Korringa Enhancement Factor in (TMTTF)$_2$PF$_6$

For investigation of the electron correlation, the Korringa enhancement factor, $K(\alpha)$, is important, which is related by,

$$T_1 T K^2 = \frac{\hbar}{4\pi k_B} K^{-1}(\alpha) \tag{39}$$
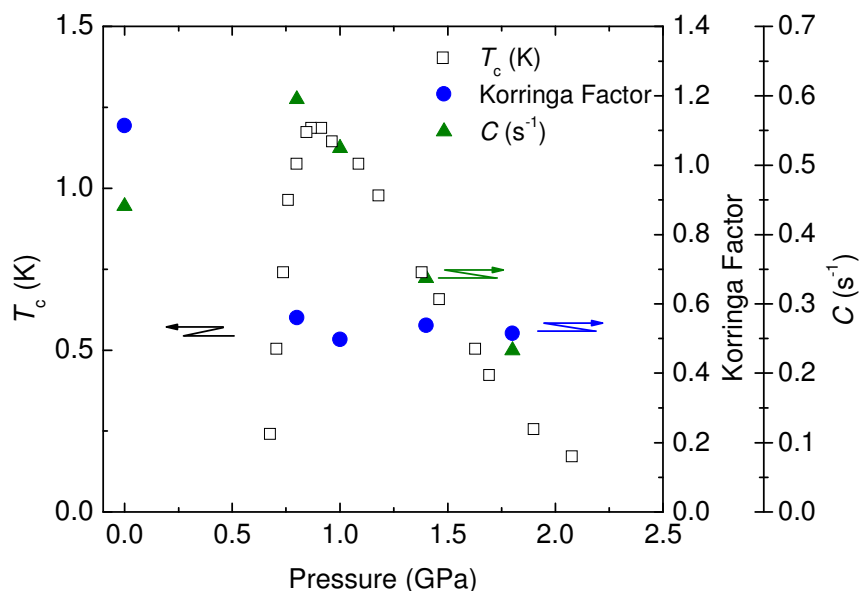
$K(\alpha)$ is the parameter depending on the electron correlation and is determined from observations of the spin-lattice relaxation time, T_1, and Knight shift, K, and other physical constants without analytical assumptions. This factor gives important information for the electron correlation. However, in case the hyperfine coupling is anisotropic, the Equation (39) is modified by the form factor and is written as,

$$T_1 T K^2 = \left(\frac{\sqrt{2}A_{//}}{A_{\perp}}\right)^2 \frac{\hbar}{4\pi k_B} K^{-1}(\alpha) \tag{40}$$

To evaluate the Korringa enhancement factor, the ratio of matrix elements in the hyperfine coupling tensor, $A_{//}/A_{\perp}$, is needed. From our hyperfine coupling tensor of (TMTSF)$_2$PF$_6$, the form factor was estimated to ~36 and the Korringa factor was estimated to ~0.55 with utilizing the observed data of the spin-lattice relaxation time, T_1, and Knight shift, K, except for SDW contribution. Figure 9 shows the pressure dependence of the Korringa factor with other parameters. This result suggested that the electron correlation except SDW fluctuation is weak as in the simple alkali metals and the Korringa factor does not change above the critical pressure of superconducting transition. Contrast to that, The

SDW fluctuation intensity, *C*, shows the same pressure dependence of T_c, suggesting the connection between superconductivity and SDW fluctuation [51].
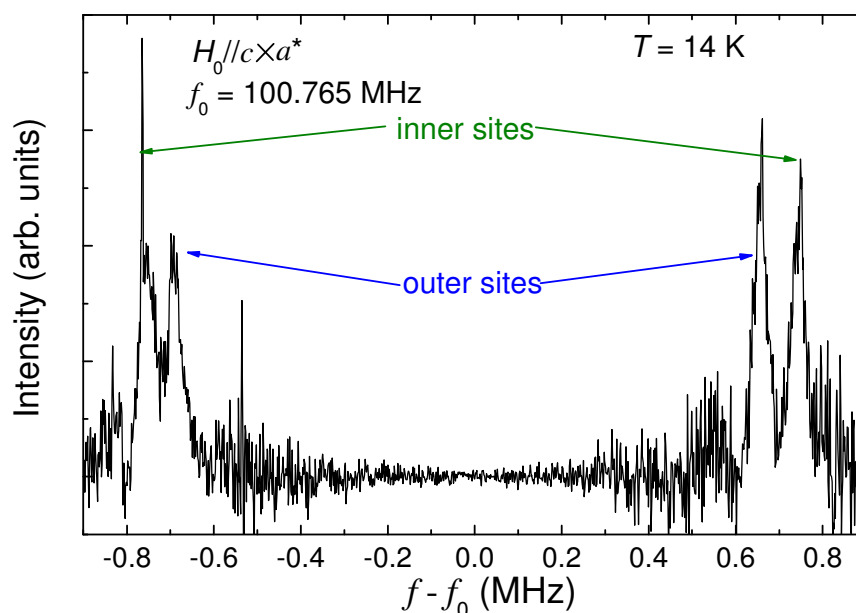
Figure 9. Pressure dependence of superconducting transition temperature, T_c, Curie-Weis expression fitting parameter, *C*, and the Korringa factor [51,55].

4.4. Determination of the Magnetic Moment in β'-(BEDT-TTF)$_2$ICl$_2$

β'-(BEDT-TTF)$_2$ICl$_2$ shows superconductivity under ultra-high pressure (8 GPa) [56]. Under ambient pressure, this salt is an insulator and undergoes an anti-ferromagnetic (AF) transition at low temperature. From the Curie constant in paramagnetic phase, the insulator phase is suggested to be a dimer Mott insulator with one local spin per a dimer [57]. It is important to verify the amplitude of the staggered moment in AF phase. We determined the hyperfine coupling tensors in ^{13}C NMR of the antiferromagnetic phase of β'-(BEDT-TTF)$_2$ICl$_2$ with single-site ^{13}C-substituted BEDT-TTF [54]. To prevent the spin-flop phenomenon, the external magnetic field was applied perpendicular to the easy axis. Thus, the antiferromagnetic moment induces the local field parallel to the external field via the off-diagonal element of the hyperfine coupling tensor. Figure 10 shows the NMR spectra with the magnetic field parallel to *b'* axis, which is perpendicular to the easy axis [57,58]. In this setting, the moment induces the internal field parallel to the quantization axis via $A_{b'c}$. In previous ^{13}C-NMR on organic conductors, the quantitative analysis was difficult due to the Pake doublet. Using hyperfine coupling tensors, however, we could perform the site assignment of spectrum shown in Figure 10, and we estimated the amplitude of the moment as ~1μ_B per dimer, predicting β'-(BEDT-TTF)$_2$ICl$_2$ under ambient pressure is a dimer Mott insulator.

Figure 10. The NMR spectra below the antiferromagnetic transition temperature at $H_0 // c \times a^*$ [54].
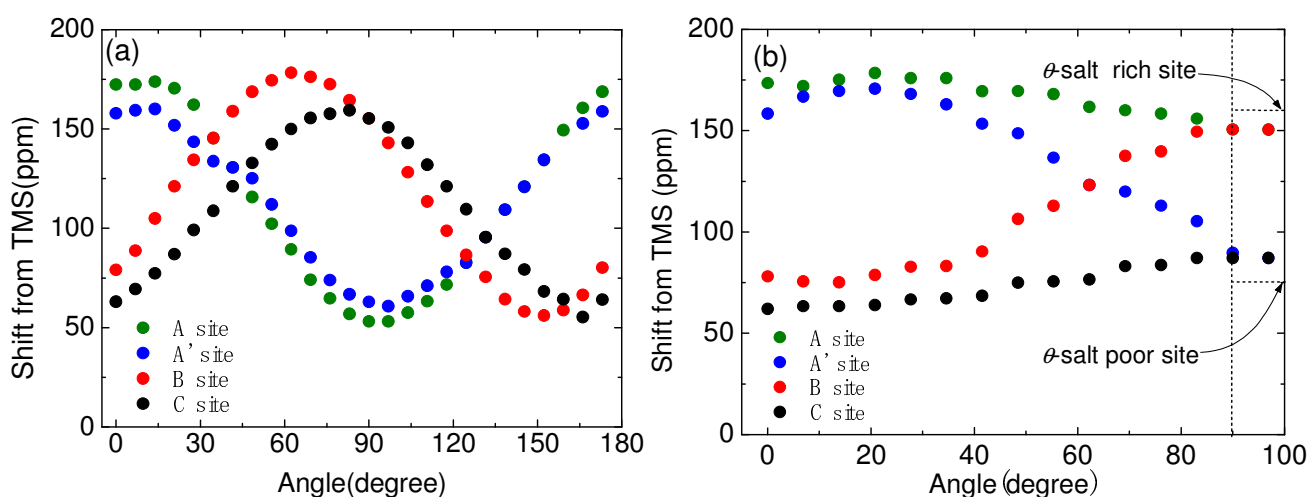

4.5. Site Assignment on Charge Order Phase in α-(BEDT-TTF)₂I₃

The α-(BEDT-TTF)$_2$I$_3$ undergoes an MI transition at 135 K and the insulator phase of this salt has been well theoretically investigated and is revealed to be a charge ordered (CO) state due to the off-site coulomb interaction. In CO state, the inversion symmetry breaking induces the charge disproportionation among two A, B, and C sites in a unit cell. The CO pattern gives important information about the electronic structure. The vibrational spectroscopy is sensitive to the electron density on the molecular orbital and one of the powerful tools for the charge disproportionation. Unfortunately, the vibrational spectroscopy can directly determine the degree of the charge disproportionation but cannot perform the site assignment [59]. The CO pattern was predicted from the molecular bond-length deduced by the precise X-ray diffraction (XRD), which is also sensitive to the electron density of bonding or anti-bonding molecular orbital. The XRD has suggested that the molecular site, C, was assigned as charge-poor site [22]. The NMR is an alternative tool for site assignment. From the angular dependence of NMR shift, NMR distinguishes the molecular sites in a unit cell [23]. Since NMR shift is expressed as the sum of Knight and chemical shift, NMR shift almost corresponds to the chemical shift in the spin singlet state. The angular dependence of the chemical shift is relative smaller than the splitting width from Pake doublet. Hence, the angular dependence of NMR shift does not show a simple sinusoidal curve but a complicated form. Previous NMR studies on double-side substituted sample reveal that the molecular site, B, is spin-poor site in metallic phase, where, because of Knight shift, the angular dependence of the NMR shift is larger than the splitting width from Pake doublet, and the angular dependence of NMR shift shows almost a sinusoidal curve. Considering the spin disproportionation in the metallic phase is precursor phenomena of the CO transition, it is suggested that the molecular site, B, is charge-poor site in CO state [23], conflicting to the conclusion from XRD.

Using a single-site ^{13}C-substituted molecule, NMR can directly probe the charge on the molecule from the chemical shift in the spin singlet state. Four peaks are observed in the single-site ^{13}C-substiuted α-(BEDT-TTF)$_2$I$_3$, and the site assignment of four observed peaks could be performed from the simple sinusoidal dependence on the in-plane rotation shown in Figure 11a. Previous NMR study of θ-(BEDT-TTF)$_2$RbZn(SCN)$_4$ suggested that the chemical shift is the most sensitive to the charge in the case of the field parallel to the molecular long axis [60]. Then, rotating the magnetic field parallel to the molecular long axis, and comparing the chemical shift with those on θ-(BEDT-TTF)$_2$RbZn(SCN)$_4$, we concluded that the molecular site, C, was assigned as charge-poor site, as suggested by XRD [22].

Figure 11. Angular dependence of the NMR shift of α-(BEDT-TTF)$_2$I$_3$ (**a**) at the magnetic field in the *ab* plane and (**b**) the magnetic field rotated around the direction perpendicular to the conducting plane and parallel to the long axis of the BEDT-TTF molecule [61].

The chemical shift tensor at charge-rich and charge-poor sites were also evaluated as,

$$\sigma_{rich} = \begin{pmatrix} \sigma_{XX} & \sigma_{XY} & \sigma_{XZ} \\ \sigma_{YX} & \sigma_{YY} & \sigma_{YZ} \\ \sigma_{ZX} & \sigma_{ZY} & \sigma_{ZZ} \end{pmatrix}_{rich} = \begin{pmatrix} 148 & 0 & 0 \\ 0 & 183 & 0 \\ 0 & 0 & 52 \end{pmatrix} \text{ (ppm)} \tag{41}$$

$$\sigma_{poor} = \begin{pmatrix} \sigma_{XX} & \sigma_{XY} & \sigma_{XZ} \\ \sigma_{YX} & \sigma_{YY} & \sigma_{YZ} \\ \sigma_{ZX} & \sigma_{ZY} & \sigma_{ZZ} \end{pmatrix}_{poor} = \begin{pmatrix} 83 & 0 & 0 \\ 0 & 168 & 0 \\ 0 & 0 & 58 \end{pmatrix} \text{ (ppm)} \tag{42}$$

respectively [61]. Here, three principle axes, *X*, *Y*, *Z*, are defined as molecular coordinates shown in the literature. Averaging these tensors, the chemical shift tensor of the charge of $\rho = 0.5e$ can be obtained as,
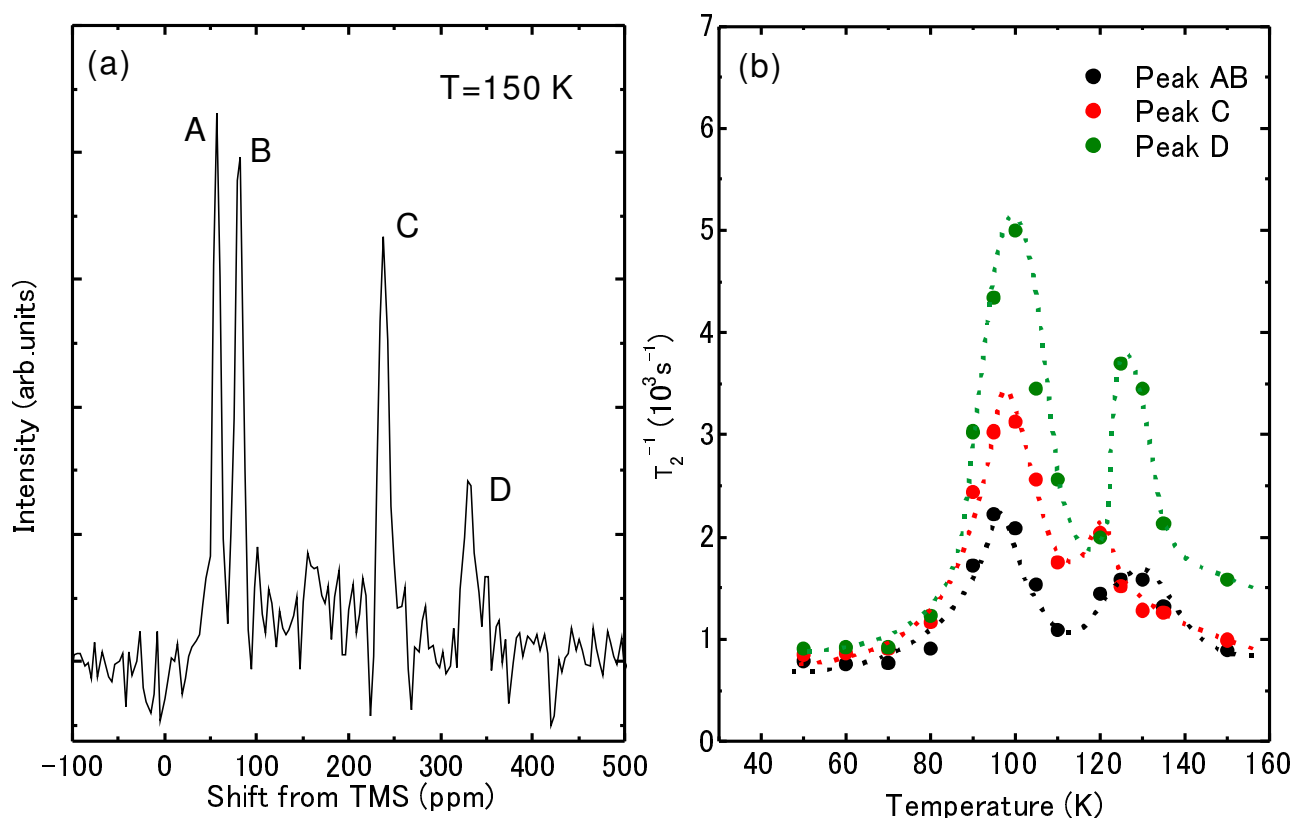
$$\sigma = \begin{pmatrix} \sigma_{XX} & \sigma_{XY} & \sigma_{XZ} \\ \sigma_{YX} & \sigma_{YY} & \sigma_{YZ} \\ \sigma_{ZX} & \sigma_{ZY} & \sigma_{ZZ} \end{pmatrix} = \begin{pmatrix} 115 & 0 & 0 \\ 0 & 175 & 0 \\ 0 & 0 & 55 \end{pmatrix} \text{ (ppm)} \tag{43}$$

The chemical shift tensor at $\rho = 0$ has been estimated using neutral molecule [62]. However, the chemical shift tensor at $\rho = 0.5e$ was unknown. The chemical shift tensor at $\rho = 0.5e$ is a basic parameter of the quantitative analysis in $(BEDT-TTF)_2X$ salts.

4.6. Slow Dynamics of Ethylene Motions in BEDT-TTF

Our previous study under various pressures revealed that κ-$(BEDT-TTF)_2Cu(NCS)_2$ shows Fermi-liquid behavior just above the superconducting transition temperature T_c, with the correlation between the Korringa factor and T_c [63]. However, this salt does not behave as a simple Fermi liquid at high temperatures. The electrical resistance of κ-$(BEDT-TTF)_2Cu(NCS)_2$ shows semiconductive behavior above 80 K and, it steeply decreases showing T^2 dependence below 30 K [64]. This behavior is a feature of all κ-type salts [15]. The anomaly in the thermal-expansion measurements at semiconductive region was found and this anomaly connected to the freezing of the ethylene motion of the BETD-TTF molecules, suggesting the glass transitions at 53 and 70 K [65]. NMR spectroscopy can detect slow dynamics corresponding to the glass transition through the spin-spin relaxation time, T_2. As the single-site ^{13}C-enriched molecule prevents the *J*-modulation by the nuclear dipole–dipole interaction, the precise measurement of T_2 can be performed, including the site dependence. Figure 12 shows the temperature dependence of T_2^{-1} at each site shown in the spectra [66]. Anomalies of the two-peak behavior were observed at around 100 and 125 K corresponding to the glass transition.

Figure 12. (a) ^{13}C NMR spectra of κ-$(BEDT-TTF)_2Cu(NCS)_2$; (b) Temperature dependence of T_2^{-1} [66].

The mechanism of the T_2 process encompasses important information for the semiconductive behavior. In the case of direct coupling caused by the dipole field of ethylene motion, T_2^{-1} is proportional to the square of the gyromagnetic ratio, γ^2, whereas, in the case of indirect coupling caused by conduction electrons, T_2^{-1} depends on one diagonal component of hyperfine coupling tensor at each site, which induces the fluctuation parallel to the external field. These anomalies of T_2^{-1} were associated with the values, not of the nuclear gyromagnetic ratio, but of the hyperfine coupling constant. Namely, T_2^{-1} at the peak D, which has a large hyperfine coupling constant, is faster than at other sites. This result provided the direct experimental evidence of the connection between the conduction electrons and the ethylene motion, and was consistent with the resulting crossover to metallic behavior when the ethylene motion freezes.

5. Conclusions

In summary, to prevent the Pake doublet problem for ^{13}C-NMR on (TMT*C*F)$_2$X and (BEDT-TTF)$_2$X, we synthesized a single-site ^{13}C-substituted TMT*C*F and BEDT-TTF molecule, utilizing the coupling of the dibutyl-tin complexes with the corresponding esters developed by Yamada *et al*. and explored an alternative method for the pure one-side enriched BEDT-TTF.

By the determination of the hyperfine coupling tensor and chemical shift tensor of TMT*C*F and BEDT-TTF, we evaluated the hyperfine coupling tensor as the basic parameter for ^{13}C-NMR of (TMT*C*F)$_2$X and (BEDT-TTF)$_2$X. These single-site ^{13}C-substituted TMT*C*F and BEDT-TTF molecules and their hyperfine coupling and chemical shift tensors enabled us to expand the ability of ^{13}C-NMR on organic conductors. We demonstrated the superiority of ^{13}C-NMR of some single-site ^{13}C-substituted molecular crystals. The preparation and basic parameters of single-site ^{13}C-substituted TMT*C*F and BEDT-TTF molecules will also contribute to future ^{13}C-NMR works.

References and Notes

1. Wang, H.H.; Beno, M.A.; Geiser, U.; Firestone, M.A.; Webb, K.S.; Nunez, L.; Crabtree, G.W.; Carlson, K.D.; Williams, J.M. Ambient-Pressure superconductivity at the highest temperature (5 K) observed in an organic system: *β*-(BEDT-TTF)$_2$AuI$_2$. *Inorg. Chem.* **1985**, *24*, 2465–2466.
2. Wang, H.H.; Geiser, U.; Williams, J.M.; Mason, J.M.; Perr, J.T.; Heindl, J.E.; Lathrop, M.W.; Love, B.J.; Watkins, D.M.; Yaconi, G.A. Phase selectivity in the simultaneous synthesis of the

T_c = 12.8 K (0.3 kbar) organic superconductor κ-(BEDT-TTF)2Cu[N(CN)2]Cl or the semiconductor (BEDT-TTF)Cu[N(CN)$_2$]$_2$. *Chem. Mater.* **1992**, *4*, 247–249.

3. Geiser, U.; Wang, H.H.; Carlson, K.D.; Williams, J.M.; Charlier, H.A.; Heindl, J.E.; Yaconi, G.A.; Love, B.J.; Lathrop, M.W.; Schirber, J.E.; *et al*. Superconductivity at 2.8 K and 1.5 kbar in κ-(BEDT-TTF)$_2$Cu$_2$(CN)$_3$: The first organic superconductor containing a polymeric copper cyanide anion. *Inorg. Chem.* **1991**, *30*, 2586–2588.

4. Urayama, H.; Yamochi, H.; Saito, G.; Nozawa, K.; Sugano, T.; Kinoshita, M.; Sato, S.; Oshima, K.; Kawamoto, A.; Tanaka, A. A new ambient pressure organic superconductor based on BEDT-TTF with T_C higher than 10 K (T_C = 10.4 K). *J. Chem. Lett.* **1988**, *17*, 55–58.

5. Jérome, D. The physics of organic superconductors. *Science* **1991**, *252*, 1509–1514.

6. Jérome, D.; Mazaud, A.; Ribault, M.; Bechgaard, K. Superconductivity in a synthetic organic conductor (TMTSF)$_2$PF$_6$. *J. Phys. Lett*. **1980**, *41*, 95–98.

7. Bechgaard, K.; Carneiro, K.; Olsen, M.; Rasmussen, F.B.; Jacobsen, C.S. Zero-Pressure organic superconductor: Di-(tetramethyltetraselenafulvalenium)-perchlorate [(TMTSF)$_2$ClO$_4$]. *Phys. Rev. Lett.* **1981**, *46*, 852–855.

8. Chow, D.S.; Zamborszky, F.; Alavi, B.; Tantillo, D.J.; Baur, A.; Merlic, C.A.; Brown, S.E. Charge ordering in the TMTTF family of molecular conductors. *Phys. Rev. Lett.* **2000**, *85*, 1698.

9. Zamborszky, F.; Yu, W.; Raas, W.; Brown, S.E.; Alavi, B.; Merlic, C.A.; Baur, A. Competition and coexistence of bond and charge orders in (TMTTF)$_2$AsF$_6$. *Phys. Rev. B* **2002**, *66*, 1–4.

10. Yu, W.; Zhang, F.; Zamborsky, F.; Alavi, B.; Baur, A.; Merlic, C.A.; Brown, S.E. Electron-Lattice coupling and broken symmetries of the molecular salt (TMTTF)$_2$SbF$_6$. *Phys. Rev. B* **2004**, *70*, 1–4.

11. Barthel, E.; Quirion, G.; Wzietek, P.; Jérome, D.; Christensen, J.B.; Jørgensen, M.; Bechgaard, K. NMR in commensurate and incommensurate spin density waves. *Europhys. Lett.* **1993**, *21*, 87–92.

12. Klemme, B.J.; Brown, S.E.; Wzietek, P.; Kriza, G.; Batail, P.; Jerome, D.; Fabre, J.M. Commensurate and incommensurate spin-density waves and a modified phase diagram of the Bechgaard salts. *Phys. Rev. Lett.* **1995**, *75*, 2408–2411.

13. Mckenzie, R.H. Similarities between organic and cuprate superconductors. *Science* **1997**, *278*, 820–821.

14. Lang, M. Quasi-Two dimensional organic superconductors. *Supercond. Rev*. **1996**, *2*, 1.

15. Kanoda, K. Electron correlation, metal-insulator transition and superconductivity in quasi-2D organic systems, (ET)$_2$X. *Phys. C* **1997**, *282–287*, 299–302.

16. Kawamoto, A.; Miyagawa, K.; Nakazawa, Y.; Kanoda, K. Electron correlation in the κ-phase family of BEDT-TTF compounds studied by ^{13}C-NMR, where BEDT-TTF is bis(ethylenedithio)tetrathiafulvalene. *Phys. Rev. B* **1995**, *52*, 15522–15533.

17. Kondo, H.; Moriya, T. Spin fluctuation-induced superconductivity in organic compounds. *J. Phys. Soc. Jpn.* **1998**, *67*, 3695–3698.

18. Kino, H.; Kontani, H. Phase diagram of superconductivity on the anisotropic triangular lattice hubbard model: An effective model of κ-(BEDT-TTF) salts. *J. Phys. Soc. Jpn*. **1998**, *67*, 3691–3694.

19. Schmalian, J. Pairing due to spin fluctuations in layered organic superconductors. *Phys. Rev. Lett.* **1998**, *81*, 4232–4235.

20. Vojta, M.; Dagotto, E. Indications of unconventional superconductivity in doped and undoped triangular antiferromagnets. *Phys. Rev. B* **1999**, *59*, 713–716.

21. Schirber, J.E.; Overmyer, D.L.; Carlson, K.D.; William, J.M.; Kini, A.M.; Wang, H.H.; Charlier, H.A.; Love, B.J.; Watkins, D.M.; Yaconi, G.A. Pressure-Temperature phase diagram, inverse isotope effect, and superconductivity in excess of 13 K in κ-(BEDT-TTF)$_2$Cu[N(CN)$_2$]Cl, where BEDT-TTF is bis(ethylenedithio)tetrathiafulvalene. *Phys. Rev. B* **1991**, *44*, 4666–4669.

22. Kakiuchi, T.; Wakabashi, Y.; Sawa, H.; Takahash, T.; Nakamura, T. Charge ordering in α-(BEDT-TTF)$_2$I$_3$ by synchrotron X-ray diffraction. *J. Phys. Soc. Jpn.* **2007**, *76*, 1–4.

23. Moroto, S.; Hiraki, K.-I.; Takano, Y.; Kubo, Y.; Takahashi, T.; Yamamoto, H.M.; Nakamura, T. Charge disproportionation in the metallic state of α-(BEDT-TTF)$_2$I$_3$. *J. Phys. IV* **2004**, *114*, 399–340.

24. Wojciechowski, R.; Yamamoto, K.; Yakushi, K.; Inokuchi, M.; Kawamoto, A. High-Pressure Raman study of the charge ordering in α-(BEDT-TTF)$_2$I$_3$. *Phys. Rev. B* **2003**, *67*, 1–11.

25. Yue, Y.; Yamamoto, K.; Uruichi, M.; Nakano, C.; Yakushi, K.; Yamada, S.; Hiejima, T.; Kawamoto, A. Nonuniform site-charge distribution and fluctuations of charge order in the metallic state of α-(BEDT-TTF)$_2$I$_3$. *Phys. Rev. B* **2010**, *82*, 1–8.

26. Bender, K.; Hennig, I.; Schweitzer, D.; Dietz, K.; Endres, H.; Keller, H.J. Synthesis, structure and physical properties of a two-dimensional organic metal, di[dis(ethylene-dithiolo)tetrathiofulvalene] triiodide, (BEDT-TTF)$^+$$_2I^-$$_3$. *Mol. Cryst. Liq. Cryst.* **1984**, *107*, 359–371.

27. Yamamoto, K.; Yakushi, K.; Miyagawa, K.; Kanoda, K.; Kawamoto, A. Charge ordering in θ-(BEDT-TTF)$_2$RbZn(SCN)$_4$ studied by vibrational spectroscopy. *Phys. Rev. B* **2002**, *65*, 1–8.

28. Miyagawa, K.; Kawamoto, A.; Kanoda, K. Charge ordering in a quasi-two-dimensional organic conductor. *Phys. Rev. B* **2000**, *62*, 7679–7682.

29. Mori, H.; Tanaka, S.; Mori, T. Systematic study of the electronic state in θ-type BEDT-TTF organic conductors by changing the electronic correlation. *Phys. Rev. B* **1998**, *57*, 12023–12029.

30. Seo, H.; Fukuyama, H. Antiferromagnetic phases of one-dimensional quarter-filled organic conductors. *J. Phys. Soc. Jpn.* **1997**, *66*, 1249–1252.

31. Seo, H. Charge ordering in organic ET compounds. *J. Phys. Soc. Jpn.* **2000**, *69*, 805–820.

32. Merino, J.; Mckenzie, R.H. Superconductivity mediated by charge fluctuations in layered molecular crystals. *Phys. Rev. Lett.* **2001**, *87*, 1–4.

33. Emery, V.J.; Bruinsma, R.; Barišić, S. Electron-Electron Umklapp scattering in organic superconductors. *Phys. Rev. Lett.* **1982**, *48*, 1039–1043.

34. Scott, J.C.; Pedersen, H.J.; Bechgaard, K. Magnetic properties of the organic conductor *bis*-tetramethyltetraselenafulvalene hexafluorophosphate [(TMTSF)$_2$PF$_6$]: A new phase transition. *Phys. Rev. Lett.* **1980**, *45*, 2125–2128.

35. Lasjaunias, J.C.; Biljaković, K.; Nad', F.; Monceau, P.; Bechgaard, K. Glass transition in the spin-density wave phase of (TMTSF)$_2$PF$_6$. *Phys. Rev. Lett.* **1994**, *72*, 1283–1286.

36. Lee, I.J.; Chow, D.S.; Clark, W.G.; Strouse, M.J.; Naughton, M.J.; Chaikin, P.M.; Brown, S.E. Evidence from [77]Se Knight shifts for triplet superconductivity in (TMTSF)$_2$PF$_6$. *Phys. Rev. B* **2003**, *68*, 1–4.

37. Takahashi, T. ^{13}C-NMR studies of charge ordering in organic conductors. *Syth. Met.* **2003**, *133–134*, 261–264.

38. Powles, J.G.; Manfield, P. Double-Pulse nuclear-resonance transients in solid. *Phys. Lett.* **1962**, *2*, 58–59.

39. Miyagawa, K.; Kawamoto, A.; Kanoda, K. ^{13}C NMR study of nesting instability in *α*-(BEDT-TTF)$_2$RbHg(SCN)$_4$. *Phys. Rev. B* **1997**, *56*, 8487–8490.

40. De Soto, S.M.; Slichter, C.P.; Kini, A.M.; Wang, H.H.; Geiser, U.; Williams, J.M. ^{13}C NMR line-shape studies of the organic superconductor *κ*-(ET)$_2$Cu[N(CN)$_2$]Br. *Phys. Rev. B* **1996**, *54*, 16101–16107.

41. Shimizu, Y.; Miyagawa, K.; Kanoda, K.; Maesato, M.; Saito, G. Emergence of inhomogeneous moments from spin liquid in the triangular-lattice Mott insulator *κ*-(ET)$_2$Cu$_2$(CN)$_3$. *Phys. Rev. B* **2006**, *73*, 140407/1–140407/4.

42. De Sono, S.M.; Slichter, C.P.; Kini, A.M.; Wang, H.H.; Geiser, U.; Williams, J.M. ^{13}C-NMR studies of the normal and superconducting states of the organic superconductor *κ*-(ET)$_2$Cu[N(CN)$_2$]Br. *Phys. Rev. B* **1995**, *52*, 10364–10368.

43. Ferraris, J.P.; Poehler, T.O.; Bloch, A.N.; Cowan, D.O. Synthesis of the highly conducting organic salt: Tetramethyltetrathiofulvalenium-tetracyano-*p*-quinodimethanide. *Tetrahedron Lett.* **1973**, *14*, 2553–2556.

44. Moradpour, A.; Peyrussan, V.; Johansen, I.; Bechgaard, K. High-Yield synthesis of tetramethyltetraselenafulvalene (TMTSF) avoiding the use of gaseous hydrogen selenide. *J. Org. Chem.* **1983**, *48*, 388–389.

45. Bechgaard, K.; Cowan, D.O.; Bloch, A.N. Synthesis of the organic conductor tetramethyltetraselenofulvalenium 7,7,8,8-tetracyano-*p*-quinodimethanide (TMTSF-TCNQ) [4,4′,5,5′-tetramethyl-Δ$^{2,2'}$-bis-1,3-diselenolium 3,6-bis-(dicyanomethylene)cyclohexadienide]. *J. Chem. Soc. Chem. Commun.* **1974**, 937–938.

46. Yamada, J.; Satoki, S.; Mishima, S.; Akashi, N.; Takahashi, K.; Masuda, N.; Nishimoto, Y.; Takasaki, S.; Anzai, H. Synthesis of unsymmetrical tetrathiafulvalene derivatives via Me$_3$Al-promoted reactions of organotin compounds with esters. *J. Org. Chem.* **1996**, *61*, 3987–3995.

47. Tetra-Methyl-Tetra-Thia-Fulvalene (TMTTF, 1). To a solution of 4,5-dimethyl-2,2-dibutyl-2-stanna-1,3-dithiole (4(a); 1600 mg, 4.56 mmol) in anhydrous dichloromethane (8.6 mL) was added at −78 °C a hexane solution of Me$_3$Al (1.08 mol/L × 9.4 mL = 10.15 mmol). And then a solution of Methyl 4,5-dimethyl-1, 3-dithiole- 2-carboxylate (5(a); 720 mg, 3.81 mmol) in anhydrous dichloromethane (8.6 mL) was added. The mixture was warmed up to room temperature, and left stirring overnight. The reaction was quenched by the addition of saturated aqueous NaHCO$_3$ solution at 0 °C. The aqueous layer was extracted with five portions of chloroform. The extracts were combined, dried over MgSO$_4$, and the solvent was evaporated in vacuo. Recrystallization of the product from acetonitrile gave 1 (TMTTF), orange crystals; yield: 360 mg (43.7%). ^{1}H-NMR (CDCl$_3$/TMS): δ = 2.01(s, 12H). MS(FD): m/z (%): 263(22), 262(15), 261(M$^+$, 100).

48. Tetra-Methyl-Tetra-Selena-Fulvalene (TMTSF, 2). To a solution of 4,5-Dimethyl-2,2-dibutyl-2-stanna-1,3-diselenole (4(b); 1361 mg, 3.06 mmol) in anhydrous dichloromethane (9.8 mL) was added at −78 °C a hexane solution of Me$_3$Al (1.08 mol/L × 5.6 mL = 6.02 mmol). And then a solution of Methyl 4,5-dimethyl-1, 3-diselenole- 2-carboxylate (5(b); 840 mg, 2.93 mmol) in

anhydrous dichloromethane (9.8 mL) was added. The mixture was warmed up to room temperature, and left stirring overnight. The reaction was quenched by the addition of saturated aqueous $NaHCO_3$ solution at 0 °C, and the mixture was filtered through Celite. The aqueous layer was extracted with three portions of chloroform. The extracts were combined, dried over $MgSO_4$, and the solvent was evaporated in vacuo. And then the product was chromatographed (silica gel, hexane- chloroform). Recrystallization of the product from acetonitrile gave 2 (TMTSF), purple crystals; yield: 100 mg (7.6%). ^{1}H-NMR ($CDCl_3$/TMS): δ = 1.98(s,12H). MS(FD): m/z (%): 455(35), 454(13), 453(84), 452(29), 451(100), 450(46), 449(M^+, 99), 448(50), 447(76), 446(42), 445(45), 444(22), 443(20).

49. Svenstrup, N.; Rasmussen, K.M.; Hansen, T.K.; Becher, J. The chemistry of TTFTT; 1: New efficient synthesis and reactions of tetrathiafulvalene-2,3,6,7-tetrathiolate (TTFTT): An important building block in TTF-syntheses. *Synthesis* **1994**, 809–812.

50. Bis-(Ethylene-Dithio)-Tetra-Thia-Fulvalene (BEDT-TTF-$^{13}C1$, 3). Enriched 2,3-Bis(cyanoethylthio)-6,7-ethylenedithiotetrathiafulvalene was prepared from the enriched thioketone form by the literature. To a solution of enriched 2,3-bis(cyanoethylthio)-6,7-ethylenedithiotetrathiafulvalene (12; 200 mg, 0.42 mmol) in degassed EtOH (10 mL) was added Sudium (40mg, 3.5mmol) in 3 mL of degassed EtOH under Ar and the mixture was stirred for 4 h. To the deep red solution was added 1,2-dibromoethane (219 mg, 1.1 mmol) in degassed EtOH (22 mL) and stirred overnight under Ar. The mixture was filtered. The product was purified by chromatography (silica gel, CS_2) and recrystallized from chlorobenzene to give 3 (BEDT-TTF-$^{13}C1$,), bright red crystals; yield: 58 mg (36%). ^{1}H-NMR ($CDCl_3$/TMS): δ = 3.27(s, 8H). MS(FD): m/z (%): 389(6), 388(5), 387(37), 386(18), 385(100), 384(3).

51. Kimura, Y.; Misawa, M.; Kawamoto, A. Correlation between non-Fermi-liquid behavior and antiferromagnetic fluctuations in (TMTSF)$_2$PF$_6$ observed using ^{13}C-NMR spectroscopy. *Phys. Rev. B* **2011**, *84*, 1–5.

52. Hirose, S.; Kawamoto, A. ^{13}C NMR study on the charge-ordering salt α'-(BEDT-TTF)$_2$IBr$_2$. *Phys. Rev. B* **2009**, *80*, 1–6.

53. Hiraki, K.; Kanoda, K.; Wigner crystal type of charge ordering in an organic conductor with a quarter-filled band: (DI-DCNQI)$_2$Ag. *Phys. Rev. Lett.* **1998**, *80*, 4737–4740.

54. Eto, Y.; Kawamoto, A. Antiferromagnetic phase in β'-(BEDT-TTF)$_2$ICl$_2$ under pressure as seen via ^{13}C NMR. *Phys. Rev. B* **2010**, *81*, 1–4.

55. Leyraud, N.D.; Senzier, P.A.; Cotret, R.S.; Bourbonnais, C.; J'erome, D.; Bechgaard, K.; Taillefer, L. Correlation between linear resistivity and T_c in the Bechgaard salts and the pnictide superconductor Ba(Fe$_{1-x}$Co$_x$)$_2$As$_2$. *Phys. Rev. B* **2009**, *80*, 1–5.

56. Taniguchi, H.; Miyashita, M.; Uchiyama, K.; Satoh, K.; Mori, N.; Okamoto, H.; Miyagawa, K.; Kanoda, K.; Hedo, M.; Uwatoko, Y. Superconductivity at 14.2 K in layered organics under extreme pressure. *J. Phys. Soc. Jpn.* **2003**, *72*, 468–471.

57. Yoneyama, N.; Miyazaki, A.; Enoki, T.; Saito, G. Magnetic properties of TTF-type charge transfer salts in the Mott insulator regime. *Bull. Chem. Soc. Jpn.* **1999**, *72*, 639–651.

58. Tokumoto, M.; Anzai, H.; Ishiguro, T.; Saito, G.; Kobayashi, H.; Kato, R.; Kobayashi, A. Electrical and magnetic properties of organic semiconductors, (BEDT-TTF)$_2$X (X = IBr$_2$, IBrCl, and ICl$_2$). *Synth. Met.* **1987**, *19*, 215–220.

59. Yamamoto, T.; Uruichi, M.; Yamamoto, K.; Yakushi, K.; Kawamoto, A.; Taniguchi, H. Examination of the charge-sensitive vibrational modes in bis(ethylenedithio)tetrathiafulvalene. *J. Phys. Chem. B* **2005**, *109*, 15226–15235.

60. Chiba, R.; Hiraki, K.; Takahashi, T.; Yamamoto, H.M.; Nakamura, T. Charge disproportionation and dynamics in θ-(BEDT-TTF)$_2$CsZn(SCN)$_4$. *Phys. Rev. B* **2008**, *77*, 1–10.

61. Kawai, T.; Kawamoto, A. ^{13}C-NMR study of charge ordering state in the organic conductor, α-(BEDT-TTF)$_2$I$_3$. *J. Phys. Soc. Jpn.* **2009**, *78*, 1–6.

62. Klutz, T.; Henning, I.; Haeberlen, U.; Schweitzer, D. Knight shift tensors and *p*-spin density in the organic metals α_t-(BEDT-TTF)$_2$I$_3$ and (BEDT-TTF)$_2$Cu(NCS)$_2$. *Appl. Magn. Reson.* **1991**, *2*, 441.

63. Itaya, M.; Eto, Y.; Kawamoto, A.; Taniguchi, H. Antiferromagnetic fluctuations in the organic superconductor κ-(BEDT-TTF)$_2$Cu(NCS)$_2$ under Pressure. *Phys. Rev. Lett.* **2009**, *102*, 1–4.

64. Strack, C.; Akinci, C.; Paschenko, V.; Wolf, B.; Uhrig, E.; Assmus, W.; Lang, M.; Schreuer, J.; Wiehl, L.; Schlueter, J.A.; *et al.* Resistivity studies under hydrostatic pressure on a low-resistance variant of the quasi-two-dimensional organic superconductor κ-(BEDT-TTF)$_2$Cu[N(CN)$_2$]Br: Search for intrinsic scattering contributions. *J. Phys. Rev. B* **2005**, *72*, 054511.

65. Müller, J.; Lang, M.; Steglich, F.; Schlueter, J.A.; Kini, A.M.; Sasaki, T. Evidence for structural and electronic instabilities at intermediate temperatures in κ-(BEDT-TTF)$_2X$ for X = Cu[N(CN)$_2$]Cl, Cu[N(CN)$_2$]Br and Cu(NCS)$_2$: Implications for the phase diagram of these quasi-two-dimensional organic superconductors. *Phys. Rev. B* **2002**, *65*, 1–14.

66. Kuwata, Y.; Itaya, M.; Kawamoto, A. Low-Frequency dynamics of κ-(BEDT-TTF)$_2$Cu(NCS)$_2$ observed by ^{13}C NMR. *Phys. Rev. B* **2011**, *83*, 1–5.